Analyst

Accepted Manuscript

This article can be cited before page numbers have been issued, to do this please use: N. Nataraj, S. K. Krishnan, T. Chen, S. M. Chen and B. Lou, *Analyst*, 2020, DOI: 10.1039/D0AN01507E.

View Article Online
DOI: 10.1039/D0AN01507E

ARTICLE

Ni-Doped ZrO_2 Nanoparticles decorated MW-CNTs nanocomposite for highly sensitive electrochemical detection of 5-Amino salicylic acid

Received 00th January 20xx,
Accepted 00th January 20xx

DOI: 10.1039/x0xx00000x

Nandini Nataraj,[a] Siva Kumar Krishnan,[b] Tse-Wei Chen,[a,c,d] Shen-Ming Chen,*[a] Bih-Show Lou*[e,f]

In this work, Ni-doped ZrO_2 nanoparticles (NPs) decorated on multi-walled carbon nanotubes (MWCNT) to obtain Ni-ZrO_2/MWCNT nanocomposite as an efficient electrode material for highly sensitive electrochemical detection of anti-inflammatory drug, 5-amino salicylic acid (5-ASA) is reported. The Ni-ZrO_2NPs was obtained through a facile, co-precipitation method, and followed by supporting of these Ni-ZrO_2NPs onto MWCNT was accomplished by ultrasonication technique. Supporting Ni-ZrO_2NPs onto MWCNTs not only possesses excellent catalytic property but also substantially enhances the surface area, electrical conductivity, and electron transfer process. The electrochemical activity of the synthesized Ni-ZrO_2/MWCNT nanocomposite was systematically investigated using cyclic voltammetry (CV) and differential pulse voltammetry (DPV) techniques. The constructed Ni-ZrO_2/MWCNT-modified glassy carbon (GC) electrode manifests superior electrocatalytic oxidation toward 5-ASA with a lower peak potential compared with the Ni-ZrO_2NPs and MWCNT-modified GC electrodes. Importantly, the proposed biosensor exhibited excellent sensitivity toward detection of 5-ASA with a wide linear concentration range (0.001-500 µM), and a lower detection limit of 0.0029 µM. Moreover, the biosensor demonstrated excellent repeatability, reproducibility, stability, and high specificity toward 5-ASA detection in the presence of different interference species. Furthermore, the biosensor showed satisfactory recovery rates in complex biological samples, such as human blood serum, human urine, and 5-ASA tablet samples.

1.Introduction

5-aminosalicylic acid (5-ASA) is also known as mesalamine or mesalazine, which is the most commonly available nonsteroid anti-inflammatory drugs widely used for treating and maintaining remission of mild to moderate inflammatory bowel diseases (IBDs), such as ulcerative colitis and Crohn's diseases.[1,2] The 5-ASA is also employed as primary treatment in the case of colorectal carcinoma,[3] and it helps in controlling active inflammation and chemoprevention of against the growth of colorectal cancer cells in patients suffering from IBDs.[4] In addition, it was evidenced that the 5-ASA is highly efficient in inhibiting bacterial peptides and reducing cell damage in the inflamed mucosa because of the presence of reactive oxygen metabolites, resulting in significant suppression in their toxicity.[5] However, overconsumption of these drugs for a prolonged period causes severe side effects, including dizziness, skin rash, stomach cramps, and vomiting.[6,7] Therefore, the development of simple, low-cost, and ultra-sensitive detection methods to accurate determination of 5-ASA is highly important in order to early-stage diagnosis. Over the past decades, a variety of analytical methods have been developed such as high-performance liquid chromatography (HPLC),[8,9] UV-vis spectrophotometric,[10] Spectrofluorometry,[11] high-performance liquid chromatography (HPLC),[8] automated chemiluminescence,[12] tandem mass spectroscopy,[13] LC-MS/MS,[14] capillary electrophoreses,[15] voltammetry methods,[16,17] for highly sensitive and specific detection of anti-inflammatory drugs. Most of these techniques require complicated equipment, and high-cost, impeding their applications in biosensors. Among all, the electrochemical platform has been considered as an efficient detection method owing to its advantages including ultra-sensitive, simple

[a] Department of Chemical Engineering and Biotechnology, National Taipei University of Technology, No.1, Section 3, Chung-Hsiao East Road, Taipei 106, Taiwan. Email: smchen78@ms15.hinet.net, smchen1957@gmail.com
[b] CONACYT-Instituto de Física, Benemérita Universidad Autónoma de Puebla, Apdo. Postal J-48, Puebla 72570, Mexico.
[c] Research and Development Center for Smart Textile Technology, National Taipei University of Technology, Taipei 106, Taiwan, ROC.
[d] Department of Materials, Imperial College London, London, SW7 2AZ, United Kingdom.
[e] Chemistry Division, Center for General Education, Chang Gung University, Taoyuan 333, Taiwan.
[f] Department of Nuclear Medicine and Molecular Imaging Center, Chang Gung Memorial Hospital, Taoyuan 333, Taiwan. Email: Email: blou@mail.cgu.edu.tw

Electronic Supplementary Information (ESI) available: EDS results, TEM images of Ni-ZrO_2/MWCNTs, Redox properties of modified GCEs, Reproducibility, Repeatability, stability analysis, Real sample analysis]. See DOI: 10.1039/x0xx00000x

View Article Online DOI: 10.1039/D0AN01975E

instrumentation and operation, rapid response, and cost-effective.[5,18]

Numerous of nanostructured metal oxides (NMOs) such as TiO_2, ZnO_2, CeO_2, SnO_2, ZnO_2, ZrO_2, etc., have gained tremendous research interest for the development of electrochemical biosensors due to their unique and desirable properties.[19–21] These NMOs provide special advantages such as size and morphology dependent electrocatalytic activities, high surface area, non-toxicity, good adsorption ability of desired analyte biomolecules, and long-term operational stability.[19]Among these NMOs, zirconium oxide nanoparticles (ZrO_2NPs) has attracted significant interest as a highly active catalytic material for the construction of biosensor electrodes for electrochemical biosening.[22–24] This is mainly because of excellent properties like good biocompatibility, chemical inertness, outstanding chemical and thermal stability, good resistance to corrosion, and high isoelectric point (~9.5).[24,25] However, low electrical conductivity, the higher tendency to an aggregation of ZrO_2NPs, significantly hinder its use in electrochemical biosensor applications.[26] To this end, doping metal cations such as Ni^{2+}, Mn^{2+}, Fe^{3+}, Co^{2+}, Cu^{2+}, and Zn^{2+} etc., with NMOs have seen to be a highly promising strategy to improve the electrical conductivity, electrochemical and catalytic properties.[27,28] In particular, Nickel (Ni) is considered to be a highly suitable dopant because of its advantages include high catalytic activity, electrochemical properties, low-cost, and environmentally friendly nature.[29,30] In specific, Zr^{4+} ions can substitute Ni^{2+} ions from the NiO lattice, promoting the strong interaction between Zr and Ni atoms, leading to enhanced electronic and catalytic activity Ni-Zr-O systems.[31,32] Numerous synthetic strategies including hydrothermal,[29,33,34] sol-gel,[32,35] sonochemical,[23] and co-precipitation route,[30] have been widely exploited for the controlled synthesis of ZrO_2NPs with tunable size and morphologies. Among all, the co-precipitation synthesis route is considered to be more efficient due to very simple process, low-temperature synthesis, high purity and homogeneity of the sample, and low-cost.[30]

In recent years, designing of hybrid nanocomposites composed of NMOs supported into a variety of matrices has been seen great promise for remarkable enhancement in the electrochemical biosensing performance.[36–39] Most commonly the hybrid nanocomposites were formed by combining metallic/metal oxide NPs with a carbon-based matrix such as carbon nanofibers (CNFs),[24] carbon nanotubes (CNTs),[40,41] and graphene (GR),[36,38,42] Among all, CNTs have been particularly attracted owing to its highly desirable properties such as high mechanical strength, chemical stability, excellent flexibility, good electrical conductivity, and biocompatibility.[17,43,44] Although, significant advances have been made by CNT based composite materials combining metallic NPs such as Silver (Ag) and gold (Au) to construct electrochemical biosensors,[45,46] stable, reproducible, and ultra-sensitive detection of anti-inflammatory drugs is still challenging. Previous studies have demonstrated that doping Ni-with ZrO_2 NPs could enhance the electrocatalytic activity, which mainly due to the synergetic effect of large amount of active sites in ZrO_2 and excellent catalytic activity of Ni.[30,32,47] Inspired by these studies, we adopted to incorporate Ni-ZrO_2NPs onto MWCNT to obtain Ni-ZrO_2/MWCNT composite, which expected to be improve the electrical and electrocatalytic properties and their performance in electrochemical biosensors.[48] For instance, *Pundir et al.*,[49] demonstrated that the utilization of ZrO_2/MWCNT nanocomposite modified electrode for electrochemical sensing of choline, which showed significant improvement in the sensitivity of the biosensor. Also, *Sadiković et al.*,[40] reported a ZrO_2/CNTs nanocomposite for electrochemical detection of nebivolol drug. However, to the best of our knowledge, no previous studies have been reported electrochemical biosensor based on Ni-ZrO_2/MWCNT nanocomposite for 5-ASA detection with high sensitivity.

In this work, we have synthesized Ni-ZrO_2/MWCNT nanocomposite and it is utilized as electrode material for construct sensitive electrochemical biosensor to 5-ASA detection. As-synthesized Ni-ZrO_2/MWCNT nanocomposite was characterized using XRD, SEM, TEM, FT-IR analysis. The electrochemical studies demonstrated that the fabricated Ni-ZrO_2/MWCNT/GCE exhibits outstanding performance in the sensing of 5-ASA with high sensitivity, selectivity, stability, and reproducibility. Finally, we have demonstrated the proposed biosensor to detect 5-ASA in real samples such as human blood serum, human urine, and commercial 5-ASA tablet samples, which is promising for practical applications.

2.Experimental

2.1 Materials.

Multiwalled carbon nanotubes (MWCNT) (95%, OD. ×ID× length = 7–15×3–6×0.5–200 µm), Zirconium chloride ($ZrCl_4$, ≥99.5 %), Nickel chloride ($NiCl_2$, 98%), oxalic acid (HO_2CCO_2H, ≥ 98%), Sodium hydroxide (NaOH, ≥ 98%), 5-aminosalicylic acid (5-ASA, ≥ 99%) were purchased from Sigma Aldrich, Taiwan. All the chemicals were used as received without any purification. The phosphate buffer solution (PBS, 0.1 M) was prepared by mixing disodium phosphate (Na_2HPO_4), and monosodium phosphate (NaH_2PO_4) and to vary the pH by adding NaOH, HCl. All the reagents and solutions were prepared using double distilled water (DDW) throughout the experiments.

2.2. Synthesis of Ni-doped ZrO_2 nanoparticles.

The Ni-ZrO_2NPs were synthesized through a facile, co-precipitation method by following a previously reported protocol with modifications.[30] In a typical synthesis, first 1.5 g of $ZrCl_4$ was added into 50 mL of DI water and allowed to magnetically stirred until a well-dispersed solution was formed. Then, 0.7 g of $NiCl_2$ is added to the above solution, and allowed to magnetically stirring for 30 min, the homogeneous solution mixture turned into a plain blue color. After that, 0.3 g of NaOH (0.15 M) was added to the above solution mixture and left undisturbed for 4 hrs. The formed Ni-ZrO_2NPs were

collected by centrifugation and subsequent washing with ethanol and DI water several times. Finally, the obtained precipitate was dried in an oven at 50°C overnight, and then the dry powder was calcined at 500°C for 2 hr. The ratio between Ni and ZrO_2 was calculated to be 2:1 based on wt% of the precursors.

2.3 Synthesis of Ni-ZrO_2/MWCNT nanocomposite.

The incorporation of Ni-ZrO_2NPs onto MWCNTs was achieved using a simple, ultrasonication technique. In a typical synthesis procedure, 1 mg of MWCNTs were dispersed in DI water using ultrasonication for 30 min, followed by the addition of 3 mg of pre-synthesized Ni-ZrO_2NPs and allowed to ultrasonication for 1 hr at room temperature. After that, the final products were washed with DI water and dried well in an oven at 50°C overnight. The obtained powder sample of Ni-ZrO_2/MWCNT nanocomposite was mechanically ground and used for further characterization studies, and to fabricate Ni-ZrO_2/MWCNT- modified GCE for electrochemical application. The overall synthesis steps involved in the formation of Ni-ZrO_2/MWCNT nanocomposite are depicted in **Scheme 1.**

2.4 Material Characterization.

The powder XRD (pXRD) spectra of the samples were obtained using a XPERT PRO X-ray diffractometer (XRD) with the Cu Kα radiation. The FT-IR spectra were acquired using a Perkin-Elmer Fourier transform infrared spectroscopy (CHI 1000 C, FT/IR-6600). The morphology and elemental analysis of the samples were studied by performing scanning electron microscopy (SEM) analysis using a field emission scanning electron microscopy (FE-SEM, A ZEISS sigma 300), and energy-dispersive X-ray spectroscopy (EDS) analysis. The electrochemical characterization was conducted by cyclic voltammetry (CV) using standard three electrodes systems, CHI 900 electrochemical workstation (CH Instruments Company, made in the USA.), and CHI. 205C and differential pulse voltammetry (DPV). The glassy carbon electrode (GCE) was used as a working electrode (working area = 0.071 cm^2), Ag/AgCl (saturated KCl) as the reference electrode, and platinum wire as the counter electrode, respectively.

2.5 Fabrication of Ni-ZrO_2/MWCNT-modified GCE.

Before fabrication of the modified electrode, the bare GCE was polished with alumina slurry until the mirror-like surface of GCE and sequentially ultrasonicated in a DI water: ethanol mixture (ratio of 1:1). To fabricate Ni-ZrO_2/MWCNT-modified GCE electrodes, 3 mg of as-synthesized Ni-ZrO_2/MWCNT powder sample was well dispersed in 1 mL of DI water using sonification for 30 min. Then, 6 µL of Ni-ZrO_2/MWCNT dispersion was drop-casted over GCE surface and allowed to dry under ambient atmosphere to obtain Ni-ZrO_2/MWCNT-modified GC electrode.

2.6 Real sample preparation.

The human blood obtained from healthy humans at Chang Gung University (CGU), was then solidified at 3°C and centrifuged at 2500 rpm for 15 min. For dilution, 1 mL of pipetted out from obtained serum and added into 25 mL of PBS (0.1 M, pH=7) without any further pretreatment, and used for the electrochemical detection of 5-ASA. The human urine sample used for real sample analysis was collected from a healthy volunteer, and it was transferred into a clean plastic container and stored in a refrigerator at 3°C. After that, urine samples were centrifuged at 6000 rpm for 15 min, and then the supernatant solution diluted with the 25 mL of PBS (01 M, pH=7.0) solution. All the experiments in blood serum and urine samples were conducted in accordance with the guidelines of Chang-Gung hospital, Taiwan and approved by the institutional review board of Chang-Gung memorial hospital (IRB NO. 201801660B), Taiwan. Informed consents were obtained from human participants of this study. For tablet sample analysis, the commercial tablet (PEN-TASA 500 mg) was purchased from a local pharmacy in Taipei city. The received tablets was ground into fine powder and then certain amount of power was dissolved in 25 mL of 0.1 M PBS and utilized for real sample measurements. The diluted samples were stored in a refrigerator until the electrochemical analysis performed.

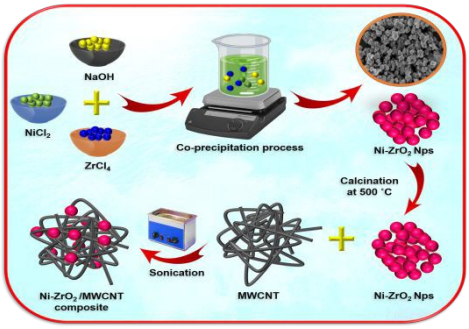

Scheme 1. Schematic representation of synthesis procedure involved to obtain Ni-ZrO_2/MWCNT nanocomposite.

3.Results and discussion

3.1 Structural and morphological characterization of Ni-ZrO_2/MWCNT nanocomposite.

X-ray diffraction (XRD) technique was employed to analyze the crystalline structure of the pristine MWCNT, Ni-ZrO_2NPs, and Ni-ZrO_2/MWCNT nanocomposite samples (**Fig. 1a**). The XRD pattern of bare MWCNT showed a characteristic diffraction peak at 2ϑ= 25.2°, assigned to the (002) planes of the graphitic structure of MWCNTs.[50] The XRD pattern of Ni-ZrO_2NPs sample exhibits major diffraction peaks at 2θ= 24.05°, 28.24°, 33.08°, 34.53°, 40.82°, 45.35°, 50.46°, 55.08°, 58.85°, 60.06°, 65.65° are indexed to the (011), (-111), (002), (020), (021), (211), (-202), (-122), (013), (031), (-302), and (222) planes of the monoclinic structure of ZrO_2NPs (JCPDS card. no. 01-0830940).[51,52] Besides these diffraction peaks, appearance of additional peaks at 2θ =31.58°, 35.31°, 38.65°, and 62.98° are associated to the (111), (200), (220), (311) planes of cubic NiO (JCPDS card. no. 040835).[30,53] After supporting Ni-ZrO_2NPs onto MWCNT, the diffraction peaks of Ni-ZrO_2NPs have existed in the diffraction pattern of Ni-ZrO_2NPs/MWCNT

View Article Online
DOI: 10.1039/D0AN01507E

nanocomposite sample (**Fig. 1a**), clearly indicates that the successful formation of Ni-ZrO_2/MWCNT nanocomposite.

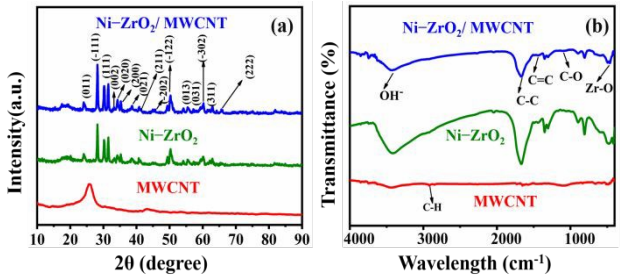

Fig. 1 (a) XRD patterns, and (b) FT-IR spectra of MWCNT, Ni-ZrO_2NPs, and Ni-ZrO_2/MWCNT nanocomposite samples.

Fourier transform-infrared spectroscopy (FT-IR) analysis was carried out to reveal the specific interaction between Ni-ZrO_2NPs and MWCNT in the Ni-ZrO_2/MWCNT nanocomposite (**Fig. 1b**). As shown in **Fig. 1b,** the FT-IR spectrum of MWCNT exhibits a broad peak at ~3450 cm^{-1} can be attributed to the stretching vibration mode of –OH groups, and less intense peaks at 2850 and 2920 cm^{-1} are assigned to the C-H stretching vibration of MWCNT.[54] The peaks at 1410, 1640, 1010 cm^{-1} are attributed to the typical stretching vibration of C=C, C-C, and C-O bonds.[54] In the FT-IR spectra of Ni-ZrO_2NPs sample, the broadband at 3400 cm^{-1} can be attributed to the stretching and bending vibration of surface adsorbed -OH groups. The other peaks between 400-990 cm^{-1}, which correspond to the starching vibration of Zr-O bond.[55] It was noticed that, similar vibrational modes of Ni-ZrO_2NPs and MWCNT have existed in the Ni-ZrO_2NPs/MWCNT composite with significant reductions in the peak intensities. These changes are ascribed to the formation of composite and existence of strong interaction between Ni-ZrO_2NPs and MWCNT in Ni-ZrO_2NPs/MWCNT nanocomposite.[54,55]

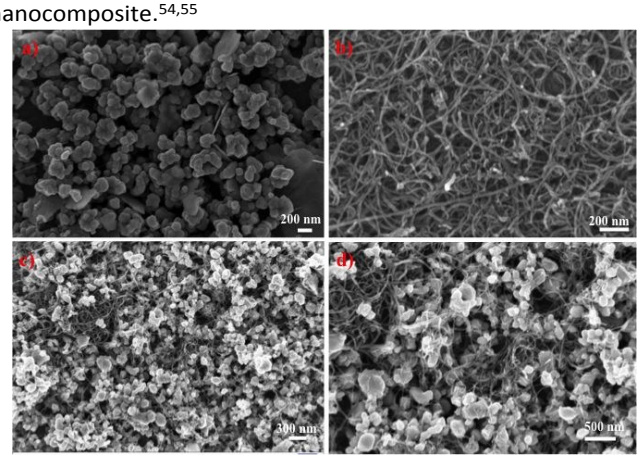

Fig. 2 FE-SEM images of (a) Ni-ZrO_2NPs, (b) MWCNT, and (c, d) Ni-ZrO_2/MWCNT nanocomposite samples.

The surface morphology of the as-synthesized samples was characterized using field emission scanning electron microscopy (FE-SEM) and transmission electron microscopy (TEM) analysis. **Fig. 2a-c** displays the FE-SEM images of the Ni-ZrO_2NPs, MWCNT, and Ni-ZrO_2/MWCNT nanocomposite samples, respectively. As shown in **Fig. 2a,** the bare Ni-ZrO_2NPs showed almost spherical-like morphology with slightly cancave and a rough surface with a particle size ranging between 200-250 nm was observed. The rough surface structure of the nanoparticles can be attributed to Ni-doping onto ZrO_2NPs, resulting in structural and morphological distortion in the final Ni-ZrO_2NPs. The SEM image of the pristine MWCNTs showed a typical one-dimensional (1D) intertwined nanotube network structure (**Fig. 2b).** The SEM image of Ni-ZrO_2/MWCNT nanocomposite in **Fig. 2c,d,** which confirmed a uniform dispersion of incorporated Ni-ZrO_2NPs onto MWCNTs. Furthermore, the uniform distribution of Ni-ZrO_2NPs onto MWCNTs was confirmed by performing the energy dispersive spectroscopy (EDX)-elemental mapping analysis (**ESI, Fig. S1a, b†**). The EDX-elemental mapping images confirmed a Zr, Ni, C, and O elements are homogeneously distributed in the resultant nanocomposite. The EDX-elemental spectrum (**ESI Fig. S1c†)** further shows the presence of only Zr, Ni, C, and O elemental peaks, and no impurities can be observed in the spectra. Moreover, the TEM images of Ni-ZrO_2NPs showed agglomerated particles of almost spherical in shape with the average size of 100-150 nm (**ESI Fig. S2 a, b†**). At the same time, the TEM image of the Ni-ZrO_2/MWCNT nanocomposite revealed that the attachment of Ni-ZrO_2NPs onto MWCNTs surface (**ESI Fig. S2 c, d†**), confirming the formation of hybrid nanocomposite.

3.2 Electrical conductivity and redox properties of various modified Electrodes.

The electrochemical impedance spectroscopy (EIS) measurements were implemented to obtain information on the bare GCE, Ni-ZrO_2NPs, MWCNT, and Ni-ZrO_2/MWCNT-modified GC electrodes as shown in **Fig. 3a**. The corresponding equivalent circuit is shown in **Fig. 3a** (inset), in which the typical Nyquist curves were fitted with the double-layer capacitance (C_{dl}), charge transfer resistance (R_{ct}), and Warburg impedance (Z_w).[56] **T**he EIS spectra of different modified-GCEs were recorded in 0.5 M KCl containing 0.1 M K_3 [$Fe(CN)_6$] and K_4[$Fe(CN)_6$]. As shown in **Fig. 3a,** typical Nyquist plots of all studied electrodes show characteristic two semicircles at high and medium frequency regions and straight-line slope in the low-frequency region. The semicircle profile at high frequencies in the spectra is attributed to the R_{ct} at the electrode-electrolyte interface.[50] As can be seen in **Fig. 3a**, the Ni-ZrO_2/MWCNT/GCE exhibits a much smaller semicircular curve when compared with the other modified electrodes. Importantly, the R_{ct} for Ni-ZrO_2/MWCNT/GCE is significantly lower (23.8 Ω) relative to those of bare GCE (266.5 Ω), Ni-ZrO_2NPs/GCE (59.7Ω), and MWCNTs/GCE (138.6 Ω). The drastically reduced R_{ct} for Ni-ZrO_2/MWCNT/GCE, suggest that the higher electrical conductivity. The enhancement in the electrical conductivity can be attributed because of the synergetic effect of both Ni-doping into ZrO_2NPs and combining them with MWCNT, which promote higher electrical conductivity in the resultant Ni-ZrO_2/MWCNT nanocomposite. Based on these results, it is evident that the constructed Ni-ZrO_2/MWCNT/GCE has lower charge transfer resistance and higher electrical conductivity, which is highly suitable for the electrochemical biosensors.

View Article Online
DOI: 10.1039/D0AN01507E

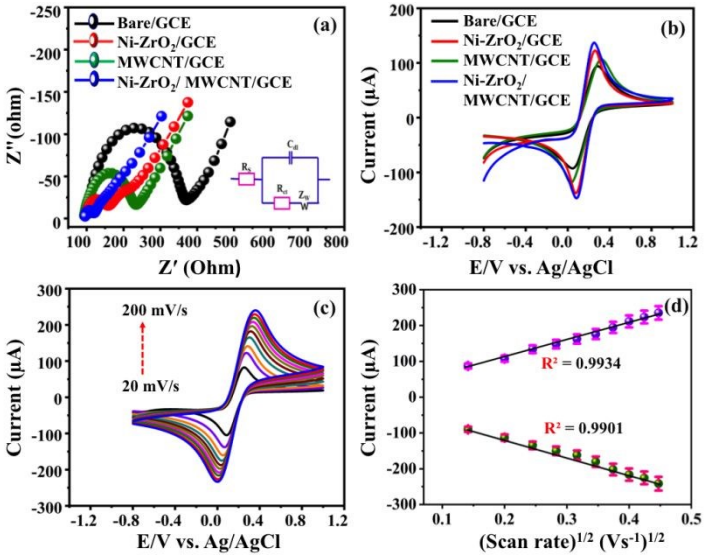

Fig. 3 (a) EIS plot of different modified GC electrodes. Inset: Randles circuit model. (b) CV curves of bare GCE, Ni-ZrO_2/GCE, MWCNT/GCE, and Ni-ZrO_2/MWCNT/GCE in 0.1 M $(Fe[CN]_6)^{3-/4-}$ containing 0.5 M of KCl, **(c)** CV curves of Ni-ZrO_2/MWCNT/GCE recorded at different scan rates in 0.1 M $(Fe\ [CN]_6)^{3-/4-}$ containing 0.5 M of KCl, (d) linear calibration plot of redox peak current *vs* square root of scan rate.

To understand the redox properties of the different modified electrodes, the cyclic voltammetry (CV) measurements were conducted in 0.1 M $[Fe(CN)_6]^{3-/4-}$ containing 0.5 M of KCl solution at a scan rate of 50 mV s^{-1} **(Fig. 3b).** As shown in **Fig. 3b,** the bare GCE and all modified GC electrodes exhibit the apparent reversible redox peaks attributed to the reversible electron transformation of $[Fe(CN)_6]^{4-}$ into $[Fe(CN)_6]^{3-}$ and also $[Fe(CN)_6]^{3-}$ into $[Fe(CN)_6]^{2-}$. It was observed that the Ni-ZrO_2NPs/MWCNT/GCE exhibited a higher reversible redox peak current (*I*p) along with the smaller peak-to-peak potential separation (ΔE_p) is about 168 mV when compared with the bare GCE, and other modified GCEs. Such high irreversible redox performance of Ni-ZrO_2/MWCNT/GCE clearly indicates that the excellent electron transfer capability during the redox process, owing to its improved available surface area in the Ni-ZrO_2/MWCNT nanocomposite. The electrochemical active surface area (EASA) of different modified GCEs was estimated using the Randles-Sevcik equation in different scan rates from 20 to 200 mV s^{-1} (**Fig. 3c**). As can be seen in **Fig 3c**, the redox peak current was gradually increased with increasing the scan rate from 20 to 200 mV. The obtained redox peak currents were fitted against the square root of scan rate (**Fig. 3d),** which showed a linear relationship. The Ni-ZrO_2/MWCNT/GCE provide a remarkably higher EASA (0.313 cm^2) relative to the bare GCE (0.080 cm^2), Ni-ZrO_2NPs/GCE (0.278 cm^2), and MWCNT/GCE (0.182 cm^2), respectively (**See ESI for more details**). Furthermore, the redox properties of bare GCE and modified electrodes were also studied in 0.1 M $Ru(NH_3)_6]^{3+/2+}$ containing 0.5 M KCl solution (See **ESI Fig. S3**†). The Ni-ZrO_2/MWCNT/GCE exhibited a higher redox current response and lower ΔE_p separation of 143 mV, relative to the bare GCE and other modified GCEs (**ESI Fig. S3a**†). In addition, the CV curves clearly show that the redox peak currents increased with increasing scan rate from 20 to 200 mV s^{-1} (**ESI Fig S3 b**†) and a linear relationship were obtained between redox current and square root of scan rate (**ESI Fig S3c**†). These results clearly suggest that the as-prepared Ni/ZrO_2/MWCNT-nanocomposite modified GCE exhibits excellent electrochemical redox activities.

3.3 Electrochemical detection of 5-ASA using Ni-ZrO_2/MWCNT/GCE.

The electrochemical performance of the bare GCE, Ni-ZrO_2/GCE, MWCNT/GCE, and Ni-ZrO_2/MWCNT/GCE was investigated using cyclic voltammetry (CV) technique. **Fig 4a** presents the CV curves of the modified electrodes in the presence of 5-ASA (75 µM) in 0.1 M PBS (pH 7.0) at a scan rate of 50 mV s^{-1}. As can be seen in **Fig. 4a**, there is no oxidation, and reduction current peaks were observed for bare GCE, whereas, the Ni-ZrO_2/GCE, MWCNT/GCE, and Ni-ZrO_2/MWCNT/GCE exhibited well-defined redox peaks. The observed quasi-reversible redox peak potential is originated from the direct electrooxidation of 5-ASA into quinone-imine (II), and reduction of quinone-imine (II) into quinone (III), through a 2 electron ($2e^-$) and 2 proton ($2H^+$) transfer process. The overall electrochemical oxidation mechanism of 5-ASA in the Ni-ZrO_2/MWCNT/GCE is illustrated in **Scheme 2.** A similar redox mechanism has been documented in the earlier studies for 5-ASA oxidation/reduction reaction, agrees with the present study.[57,58] Moreover, the redox peak current for Ni-ZrO_2/MWCNT/GCE is about 10.33 µA, which is higher than that of the Ni-ZrO_2/GCE (8.57 µA), and MWCNTs/GCE (7.49 µA), respectively (**Fig. 4b**).

View Article Online
DOI: 10.1039/D0AN01507E

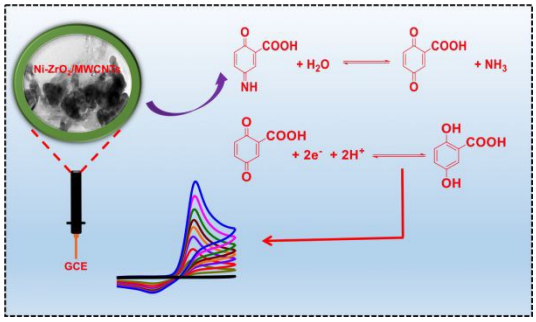

Scheme 2. Electrochemical oxidation mechanism of 5-ASA.

These results indicate that the Ni-ZrO_2/MWCNT/GCE has superior electrocatalytic activity and efficient mediator to detect 5-ASA in comparison with the other modified electrodes. The enhanced electrocatalytic activity could be ascribed to the doping catalytically active Ni onto ZrO_2, provide a large number of active sites, improved the surface area, and electrical conductivity. In addition to that, supporting Ni-ZrO2NPs onto MWCNT further boosts the electrocatalytic performance, and electron transfer kinetics during electrocatalytic oxidation of 5-ASA.

The superior electrochemical performance of the Ni-ZrO_2/MWCNT/GCE was further investigated by recording the CV curves with the consecutive injection of various concentrations of 5-ASA in 0.1 M PBS (pH= 7.0) at a scan rate of 50 mVs^{-1}. As displayed in **Fig. 4c**, the peak current is gradually increased when the 5-ASA concentrations raised from 0-200 µM. Furthermore, excellent linearity between the peak current as a function of 5-ASA concentrations was observed with a correlation coefficient of R^2=0.9942 (**Fig. 4d**). These results confirm that the excellent electrochemical activity of Ni-ZrO_2/MWCNT/GCE, and capable of detecting 5-ASA over a wide concentration range.

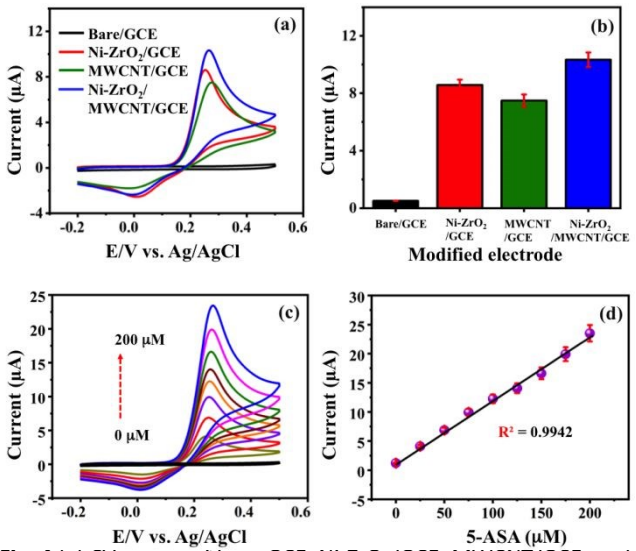

Fig. 4 (a) CV curves of bare GCE, Ni-ZrO_2/GCE, MWCNT/GCE, and Ni-ZrO_2/MWCNT/GCE in the presence of 0.1 M PBS (pH= 7.0) containing 75 µM 5-ASA at a scan rate of 50 mV s^{-1} (b) Corresponding bar diagram of I_{pa} versus modified electrodes, (c) CV response of the Ni-ZrO_2/MWCNT/GCE with various concentrations of 5-ASA (0-200 µM) in 0.1 M PBS (pH=7.0) at a scan rate of 50 mV s^{-1}, (d) Calibration plots of peak current values *vs* 5-ASA concentration.

3.4 Effect of Scan rate and pH at Ni-ZrO_2/MWCNT/GCE.

The optimizations of the electrochemical parameters such as scan rate and pH are highly essential for the electrochemical biosensors. Therefore, the CV curves were recorded by varying scan rates from 50 to 500 mV s^{-1} in 0.1 M PBS containing 5-ASA (75 µM), as shown in **Fig. 5a**. It was observed that the anodic peak current response is linearly increased along with the peak potentials shifted towards a more positive direction with increasing the scan rate from 50 to 500 mV s^{-1} (**Fig. 5a**). In addition, a good linear relationship between peak current response and square root of scan rate from 50 to 500 mVs^{-1} was obtained (**Fig. 5b)**. The observed linearity equations were well defined as with their regression equation y = 0.3299 x + 1.5509, and the correlation coefficient as R^2 = 0.9935, suggesting that the involvement of diffusion-controlled electrochemical process of 5-ASA oxidation on Ni-ZrO_2/MWCNT/GCE.[59]

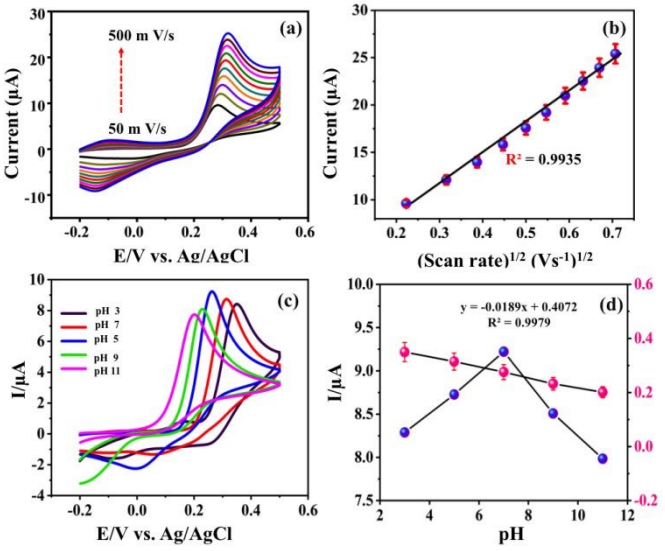

Fig. 5 (a) CVs curves of the Ni-ZrO_2/MWCNT/GCE at different scan rates from 50 to 500 mV s^{-1} in 0.1 M PBS containing 75 µM of 5-ASA. (b) The linear calibration plot of peak current *vs* square root of scan rate. (c) CV curves of the biosensor at various pH values from 3.0 to 11.0 in 0.1 M PBS containing 75 µM of 5-ASA with a sweep rate of 50 mV s^{-1}. (d) Corresponding peak current and peak potential *vs.* pH.

View Article Online
DOI: 10.1039/D0AN01507E

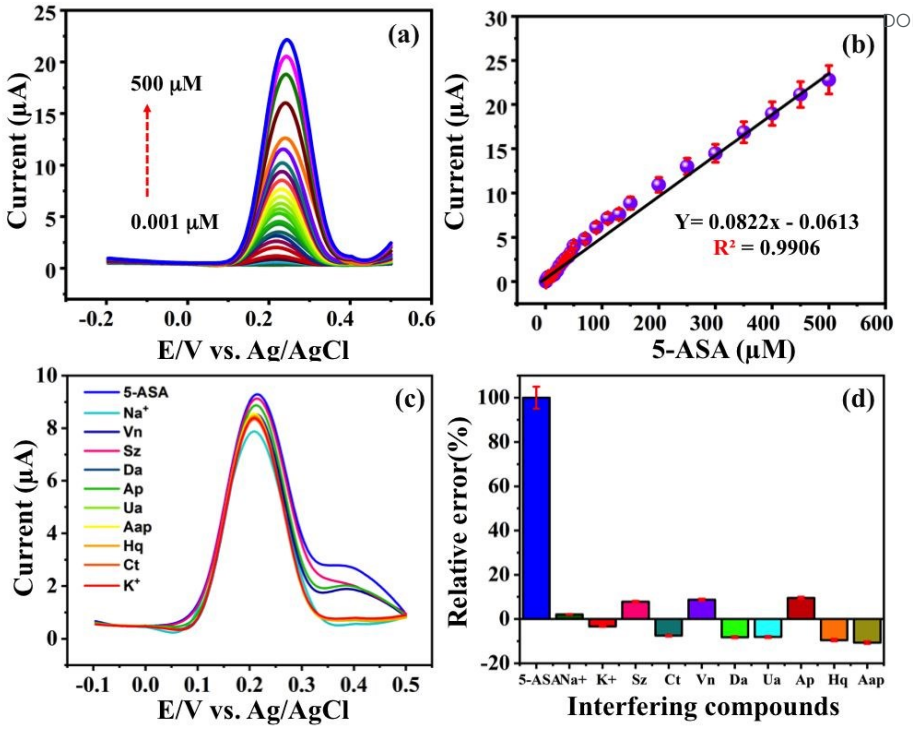

Fig. 6 (a) DPV current response of Ni-ZrO_2/MWCNT/GC electrode with various concentrations of 5-ASA ranging from 0.001-500 µM in 0.1 M PBS. (b) Dependence of peak current *vs* 5-ASA concentration. (c) DPV profiles of Ni-ZrO_2/MWCNT/GCE in the presence of different interfering species. Inset: shows the magnified image the maximum peak current positions, and (d) Bar chart diagram of the relative error *vs* various interfering species.

In addition, the pH of the electrolyte solution (PBS, 0.1 M) subjected to the electrochemical measurements can affect the electrochemical responses, such as the shape of CV curves and the peak potential of the modified electrode. Therefore, to understand the impact of pH value of PBS (0.1 M), CV response curves were recorded at various pH values from 3.0 to 11.0 in the presence of 75 µM, 5-ASA at a fixed scan rate of 50 mV s^{-1}. As shown in **Fig. 5c**, when increases the pH values from 3.0 to 11.0, the peak potentials were shifted linearly toward lower potential values, suggest that the direct participation of proton in the current-determining process.[5,57] Moreover, the peak current of 5-ASA is increased up to pH=7.0, and further increases the pH above 7.0, the peak current is found to be decreasing (**Fig. 5d**). In the measured pH range, the maximum peak current value was achieved at pH= 7.0; therefore, the pH= 7.0 was designated for the electrochemical measurements of 5-ASA detection. In addition, a linear relationship between peak potential and pH was observed (**Fig 5d**). The number of electrons involved in the oxidation reaction was estimated using the following equation:

$$E=E_0-0.0591pH/n \quad \text{.....} \quad (1)$$

Where *E* is the peak potential, E_0 is the formal potential, and n is the number of transferred electrons in the oxidation process. By substituting the above values, the number of electrons transferred is estimated to be 2 during the oxidation reaction as illustrated in **scheme 2**.

3.5 DPV detection of 5-ASA at Ni-ZrO_2/MWCNT/GCE.

In comparison with the CV, the DPV detection technique is considered to be highly sensitive and high-resolution analytical method to accurate determination of analyte molecules. Therefore, DPV measurement was implemented to evaluate biosensor performance and low detection limit (LOD) to 5-ASA detection. **Fig. 6a** displays the DPV response of Ni-ZrO_2/MWCNT/GCE to the detection of 5-ASA concentrations ranging between 0.001-500 µM in N_2-saturated 0.1 M PBS solution. As can be noticed in **Fig. 6a**, the Ni-ZrO_2/MWCNT/GCE showed a fast response when the successive addition of 5-ASA concentration ranging between 0.001 to 500 µM. Notably, the dependence of anodic peak current (I_{pa}) versus 5-ASA concentration found to be linearly increased from 0.001 to 500 µM as can be witnessed in the linear plot in **Fig. 6b**. The linear regression equation of I_{pa} (µA)= 0.0822 (µM) + 0.0613 and the coefficient R^2= 0.9906 for 5-ASA concentration ranging between 0.001-500 µM was observed. The LOD of the Ni-ZrO_2/MWCNT/GCE was estimated to be 0.0029 µm using the following standard equation:

$$LOD = 3 (S_D/S) \text{ ----------} \quad (2)$$

Where S is the slope value (0.0822 µA μM^{-1}) obtained from the linear plot in **Fig 6b**, and S_D is the standard deviation of blank current response for three measurements is about 0.0000816 µA

View Article Online DOI: 10.1039/D0AN01507F

(**ESI, Fig S4†).** To confirm the superior performance of the proposed biosensor, the sensing performance was compared with earlier reports on electrode constructed with different metal oxide nanostructures, and metal oxides supported CNTs/GR composite materials for electrochemical determination of 5-ASA as summarized in **Table 1**. According to the results presented in table 1, the fabricated biosensor showed higher analytical values such as linear range, and LOD toward electrochemical detection of 5-ASA. The enhanced performance of the biosensor can be attributed because of the synergetic effect of Ni-ZrO_2NPs and MWCNT, both of these counterparts significantly enhance the available surface area, and electrical conductivity of the Ni-ZrO_2/MWCNT nanocomposite, resulting in high sensitivity, and low LOD to electrochemical detection of 5-ASA.

3.6 Selectivity of Ni-ZrO_2/MWCNT/GCE for detection of 5-ASA

The specificity is an essential analytical parameter for the electrochemical biosensor to discriminate among different interfering species and the target analyte molecules. Hence, the selectivity of the modified electrode was accessed using DPV under optimized experimental conditions. The selective determination of 5-ASA was performed with the presence of potential interfering species such as sodium ions (Na^+), Vanillin (Vn), Sulfasalazine (Sz), dopamine (DA), Aspirin (Ap), uric acid (UA), acetaminophen (Aap), hydroquinone (Hq), catechol (CT), potassium ions (K^+). **Fig. 6c** displays the DPV response of 5-ASA (75μM) detection using Ni-ZrO_2/MWCNT/GCE in the presence of 10-fold excess concentrations of above-mentioned interference substances in N_2-saturated 0.1 M PBS. As shown in **Fig. 6c**, there are no apparent change in the DPV current responses of 5-ASA was observed in the presence of different interference species. **Fig. 6d** shows the relative error plot for detection of 5-ASA containing a 10-fold concentration of various interferences, which revealed that the interfering compounds exhibit a relative error in the range of 1-10%. In contrast, the DPV signal of 5-ASA was found to be 100% than the signals of those interference species. The high relative error of 5-ASA responses can be attributed to the strong affinity of the 5-ASA molecules onto Ni-ZrO_2/MWCNT nanocomposite surface. These results indicate that the excellent anti-interference ability of the proposed biosensor toward 5-ASA detection.

3.7 Reproducibility, repeatability, stability studies of Ni ZrO_2/MWCNT/GCE.

The reproducibility, repeatability, operational stability is a crucial parameter of the biosensor, which usually limits the practical applicability of the biosensor. Hence, the reproducibility of the modified electrode was verified by measuring five-different independent electrodes in the presence of 5-ASA (75 μM) containing N_2-saturated 0.1 M PBS. The results from five-different modified electrodes displayed the same DPV response with a slight difference in their current values, indicates that the excellent reproducibility of the biosensor (**ESI Fig. S5a†).** Next, the repeatability test was examined by using the single modified electrode for 5-ASA detection for seven repeated measurements, as shown in (**ESI Fig. S5b†**). The results showed no noticeable change in the DPV current response upto 7th repeated measurements, suggest that the appreciable repeatability. Finally, the operational stability of the electrode was also inspected to evaluate the long-term stability of the modified electrode. The stability measurements were conducted by storing the modified electrode at 4°C, and the DPV current response of 5-ASA (75 μM) was recorded for every five-days period under identical conditions up to 25 days. After consecutive measurements in each 5-days gap over 25 days, the modified electrode retained the DPV current about 98% of its initial current value (**ESI Fig. S5c†**), indicating that the excellent long-term stability of the proposed biosensor. These results confirm that the proposed biosensor has excellent

Table 1. Comparison of biosensor performance with the earlier reported of different metal oxide-based biosensors for electrochemical detection of 5-ASA.

Modified electrode	Detection technique	LOD (μM)	Linear range (μM)	Ref.
CTAB/Graphite paste	CV	0.0019	60-140	[59]
Nafion-CNT/GCE	SWV	0.11	0.5-10	[17]
Chitosan/CNT/GCE	SWV	0.21	1-18	[44]
Pencil graphite	SWV	0.0212	0.978-72.5	[60]
β-cyclodextrin/rGO/GCE	DPV	0088	0.04-13.0	[61]
GO/molecular imprinted polymers/GCE	DPV	0.97	2-20	[62]
Graphene	Microfluidic	0.50	1-20	[63]
Poly(analine)/Carbon paste	CV	0.23	20-180	[64]
$SrSnO_3$/GCE	DPV	0.002	0.01-212	[57]
Ni-ZrO_2/MWCNT/GCE	DPV	0.0029	0.001-500	this work

View Article Online
DOI: 10.1039/D0AN01507E

reproducibility, repeatability, and stability performance, suggesting that the potential suitability for the analytical applications.

3.8 Real sample analysis.

The biosensor performance in a more complex biological environment is highly essential for their practical application. Therefore, the biosensor performance was investigated in real samples such as human blood serum, urine, and commercial 5-ASA tablet samples by spike and recovery experiments using DPV technique. Briefly, the human blood serum and urine samples were diluted in 25 mL of 0.1 M PBS (See experimental section for more details), and the known concentration of 5-ASA was spiked, and the corresponding DPV response was recorded. The modified electrode showed the DPV curves exhibit the oxidation peaks of 5-ASA at their respective peak potential values, and the I_{pa} increased linearly with increasing concentration of 5-ASA ranging between 0-100 μM for both blood serum and urine samples (**ESI Fig. S6a-d†**). For conventional 5-ASA tablet sample, the I_{pa} increased linearly with increasing concentration of 5-ASA ranging between 0-80 μM (**ESI Fig. S6e, f†**). The real sample analysis in the human blood, human urine, and 5-ASA tablets revealed that the negligible matrix effects even though the concentration of real sample was higher, indicating high specificity of the proposed biosensor. **Table 2** summarizes the experimental results of found and recovery values estimated by spiking specific concentrations of 5-ASA. The recovery of 5-ASA in human blood, urine, and 5-ASA tablet samples varied from 95.92 to 99.92%, while the RSDs is changed from 3.25% to 4.9%. These results suggest that the proposed biosensor exhibits an acceptable range of recovery values, demonstrates that the biosensor can be used for practical applications in clinical samples.

Table 2: Real sample analysis in human blood, urine and 5-ASA tablet at Ni-ZrO_2/WCNT/GCE.

Real Sample	Added* (μM)	Detected [a] (μM) DPV	Recovery (%)	RSD*
Human blood	25	24.97	99.88	3.25
	50	49.25	98.5	4.65
	75	74.06	98.74	4.9
	100	98.72	98.78	4.45
Human Urine	25	24.34	97.36	3.4
	50	49.58	99.16	4.4
	75	74.95	99.03	4.7
	100	99.9	99.1	3.5
5-ASA Tablet	25	23.98	95.92	4.36
	50	49.08	98.18	3.39
	75	74.67	99.56	3.9
	100	99.92	99.71	4.28

*Relative standard deviation

4. Conclusions

In summary, we have demonstrated an electrochemical biosensor based on Ni-ZrO_2/MWCNT nanocomposite for highly sensitive determination of an anti-inflammatory drug, 5-ASA. It was found that the supporting Ni-ZrO_2NPs in the resultant Ni-ZrO_2/MWCNT nanocomposite exhibits greatly enhanced surface area, electrical conductivity and electrochemical oxidation activity toward 5-ASA in comparison with the Ni-ZrO_2NPs and MWCNT. Thus, the synergetic effect of each component in Ni-ZrO_2/MWCNT nanocomposite enabled an outstanding electrochemical performance toward sensing of 5-ASA. The Ni-ZrO_2/MWCNT/GCE manifests higher sensitivity, wide linear range (0.001-500 μM), and LOD of 0.0029 μM for 5-ASA detection. Moreover, the biosensor showed excellent selectivity, stability, and reproducibility toward the sensing of 5-ASA. Finally, the potential use of the biosensor was examined and validated in real samples such as human blood serum, human urine, and 5-ASA tablet samples, which demonstrated a satisfactory recovery rates. The synthesis route afforded to obtain Ni-ZrO_2/MWCNT nanocomposite and their superior electrochemical performance offer a promising opportunity for the sensitive electrochemical platform to detect various anti-inflammatory drugs for their clinical applications.

Conflicts of interest

"There are no conflicts to declare".

Acknowledgements

The authors gratefully acknowledge the financial support of the Ministry of Science and Technology, Taiwan through contract nos. MOST108-2221-E-182-030 and MOST 107-2113-M-027-005-MY3. The financial support from the Chang Gung Memorial Hospital through contract no. CMRPD5H0032 to B.S. Lou is also acknowledged.

Notes and references

1 K. Yeshi, R. Ruscher, L. Hunter, N. L. Daly, A. Loukas and P. Wangchuk, *Clin. Med.*, 2020, **9**, 1273–1312.
2 G. Frieri, M. T. Pimpo, A. Andreoli, V. Annese, M. Comberlato, G. Corrao, G. Palumbo, G. C. Sturniolo, F. Tonelli and R. Caprilli, *Aliment. Pharmacol. Ther.*, 1999, **13**, 577–582.
3 W. Kruis, E. Schütz, P. Fric, B. Fixa, G. Judmaier and M. Stolte, *Aliment. Pharmacol. Ther.*, 1997, **11**, 853–858.
4 M. Iacucci, S. De Silva and S. Ghosh, *Can. J. Gastroenterol.*, 2010, **24**, 127–133.
5 J. Vinoth Kumar, T. Kokulnathan, S. M. Chen, T. W. Chen, A. M. Elgorban, M. S. Elshikh, N. Marraiki and E. R. Nagarajan, *ACS Sustain. Chem. Eng.*, 2019, **7**, 18279–18287.
6 L. A. Christensen, J. Fallingborg, B. A. Jacobsen, K. Abildgaard, H. H. Rasmussen, S. H. Hansen and S. N. Rasmussen, *Aliment. Pharmacol. Ther.*, 1994, **8**, 289–294.
7 B. Norlander, R. Gotthard and M. Strom, *Aliment. Pharmacol. Ther.*, 1990, **4**, 497–505.

8 G. Palumbo, S. Bacchi, L. Primavera, P. Palumbo and G. Carlucci, *Biomed. Chromatogr.*, 2005, **19**, 350–354.
9 M. S. Elmasry, I. S. Blagbrough, M. G. Rowan, H. M. Saleh, A. A. Kheir and P. J. Rogers, *J. Pharm. Biomed. Anal.*, 2011, **54**, 646–652.
10 K. M. Patel, C. N. Patel, B. Panigrahi, A. S. Parikh and H. N. Patel, *J. Young Pharm.*, 2010, **2**, 284–288.
11 F. L. Cui, L. X. Qin, F. Li and H. X. Luo, *J. Mol. Model.*, 2008, **14**, 1111–1117.
12 E. J. Llorent-Martínez, P. Ortega-Barrales, M. L. Fernández De Córdova and A. Ruiz-Medina, *Anal. Bioanal. Chem.*, 2009, **394**, 845–853.
13 E. Pastorini, M. Locatelli, P. Simoni, G. Roda, E. Roda and A. Roda, *J. Chromatogr. B Anal. Technol. Biomed. Life Sci.*, 2008, **872**, 99–106.
14 J. Qin, X. Di, X. Wang and Y. Liu, *Biomed. Chromatogr.*, 2015, **29**, 261–267.
15 X. Zhang, Y. Xuan, A. Sun, Y. Lv and X. Hou, *Luminescence*, 2009, **24**, 243–249.
16 M. Štěpánková, R. Šelešovská, L. Janíková and J. Chýlková, *Chem. Pap.*, 2017, **71**, 1419–1427.
17 B. Nigović, M. Sadiković and S. Jurić, *Talanta*, 2016, **147**, 50–58.
18 T. Kokulnathan, T.-J. Wang, E. A. Kumar, V. Suvina and R. G. Balakrishna, *ACS Appl. Nano Mater.*, 2020, **3**, 4522–4529.
19 Y. B. Hahn, R. Ahmad and N. Tripathy, *Chem. Commun.*, 2012, **48**, 10369–10385.
20 J. M. George, A. Antony and B. Mathew, *Microchim. Acta*, 2018, **185**, 358–384.
21 A. Fallatah, M. Almomtan and S. Padalkar, *ACS Sustain. Chem. Eng.*, 2019, **7**, 8083–8089.
22 S. Kumar, S. Kumar, S. Tiwari, S. Srivastava, M. Srivastava, B. K. Yadav, S. Kumar, T. T. Tran, A. K. Dewan, A. Mulchandani, J. G. Sharma, S. Maji and B. D. Malhotra, *Adv. Sci.*, 2015, **2**, 1500048–1500057.
23 T. W. Chen, A. Sivasamy Vasantha, S. M. Chen, D. A. Al Farraj, M. Soliman Elshikh, R. M. Alkufeidy and M. M. Al Khulaifi, *Ultrason. Sonochem.*, 2019, **59**, 104718–104726.
24 T. Kokulnathan, T. S. K. Sharma, S.-M. Chen and Y. Han-Yu, *J. Electrochem. Soc.*, 2018, **165**, B281–B288.
25 P. P. Sharma, P. K. Gupta and P. R. Solanki, *Adv. Sci. Lett.*, 2018, **24**, 873–880.
26 P. K. Gupta, D. Chauhan, Z. H. Khan and P. R. Solanki, *ACS Appl. Nano Mater.*, 2020, **3**, 2506–2516.
27 P. K. Gupta, Z. H. Khan and P. R. Solanki, *J. Electroanal. Chem.*, 2018, **829**, 69–80.
28 E. W. McFarland and H. Metiu, *Chem. Rev.*, 2013, **113**, 4391–4427.
29 T. Al-Harbi, *J. Alloys Compd.*, 2011, **509**, 387–390.
30 G. Rajesh, S. Akilandeswari, D. Govindarajan and K. Thirumalai, *Mater. Res. Express*, 2019, **6**, 1050a9-1050a24.
31 Y. Wu, J. Gao, Y. He and T. Wu, *Appl. Surf. Sci.*, 2012, **258**, 4922–4928.
32 J. S. Valente, M. Valle-Orta, H. Armendáriz-Herrera, R. Quintana-Solórzano, P. Del Angel, J. Ramírez-Salgado and J. R. Montiel-López, *Catal. Sci. Technol.*, 2018, **8**, 4070–4082.
33 W. Cao, J. Kang, G. Fan, L. Yang and F. Li, *Ind. Eng. Chem. Res.*, 2015, **54**, 12795–12804.
34 L. Kumari, G. H. Du, W. Z. Li, R. S. Vennila, S. K. Saxena and D. Z. Wang, *Ceram. Int.*, 2009, **35**, 2401–2408.
35 M. R. H. Siddiqui, A. I. Al-Wassil, A. M. Al-Otaibi and R. M. Mahfouz, *Mater. Res.*, 2012, **15**, 986–989.
36 R. Karthik, J. Vinoth Kumar, S. M. Chen, C. Karuppiah, Y. H. Cheng and V. Muthuraj, *ACS Appl. Mater. Interfaces*, 2017, **9**, 6547–6559.
37 D. M. Stanković, M. Ognjanović, M. Jović, V. Cuplić, A. Lesch, H. H. Girault, M. Gavrović Jankulović and B. Antić, *Electroanalysis*, 2019, **31**, 1534–1542.
38 S. A. Alkahtani, A. M. Mahmoud, M. H. Mahnashi, R. Ali and M. M. El-Wekil, *Biosens. Bioelectron.*, 2020, **150**, 111849–111855.
39 B. Muthukutty, A. Krishnapandi and S. M. Chen, *New J. Chem.*, 2020, **44**, 2489–2499.
40 M. Sadiković and B. Nigović, *Int. J. Electrochem. Sci.*, 2017, **12**, 9675–9688.
41 Z. Sun, X. Zhang, N. Na, Z. Liu, B. Han and G. An, *J. Phys. Chem. B*, 2006, **110**, 13410–13414.
42 S. Kumar, J. G. Sharma, S. Maji and B. D. Malhotra, *Biosens. Bioelectron.*, 2016, **78**, 497–504.
43 V. Schroeder, S. Savagatrup, M. He, S. Lin and T. M. Swager, *Chem. Rev.*, 2019, **119**, 599–663.
44 B. Nigović, A. Mornar, E. Brusač and M. L. Jeličić, *J. Electroanal. Chem.*, 2019, **851**, 113450–113458.
45 S. Alim, J. Vejayan, M. M. Yusoff and A. K. M. Kafi, *Biosens. Bioelectron.*, 2018, **121**, 125–136.
46 L. A. Goulart, R. Gonçalves, A. A. Correa, E. C. Pereira and L. H. Mascaro, *Microchim. Acta*, 2018, **185**, 185–194.
47 V. M. Gonzalez-Delacruz, R. Pereñiguez, F. Ternero, J. P. Holgado and A. Caballero, *ACS Catal.*, 2011, **1**, 82–88.
48 M. Romero-Sáez, A. B. Dongil, N. Benito, R. Espinoza-González, N. Escalona and F. Gracia, *Appl. Catal. B Environ.*, 2018, **237**, 817–825.
49 S. Pundir, N. Chauhan, J. Narang and C. S. Pundir, *Anal. Biochem.*, 2012, **427**, 26–32.
50 M. Keerthi, G. Boopathy, S. M. Chen, T. W. Chen and B. S. Lou, *Sci. Rep.*, 2019, **9**, 1–12.
51 M. Jafarpour, E. Rezapour, M. Ghahramaninezhad and A. Rezaeifard, *New J. Chem.*, 2014, **38**, 676–682.
52 S. Bajpai, S. Singh and V. Srivastava, *Synth. Commun.*, 2017, **47**, 1514–1525.
53 S. Rakshit, S. Ghosh, S. Chall, S. S. Mati, S. P. Moulik and S. C. Bhattacharya, *J. Mater. Chem. C*, 2013, **3**, 19348–19356.
54 K. Ghosh, S. K. Srivastava and S. Puravankara, *J. Nanosci. Nanotechnol.*, 2019, **19**, 3367–3375.
55 M. N. Yazdi, Y. Yamini and H. Asiabi, *J. Chromatogr. A*, 2018, **1554**, 8–15.
56 S. Ebrahimi, A. Afkhami and T. Madrakian, *J. Electroanal. Chem.*, 2019, **838**, 186–194.
57 B. Muthukutty, R. Karthik, S. M. Chen and M. Abinaya, *New J. Chem.*, 2019, **43**, 12264–12274.
58 R. K. Palsmeier, D. M. Radzik and C. E. Lunte, *Pharm. Res. An Off. J. Am. Assoc. Pharm. Sci.*, 1992, **9**, 933–938.
59 A. Nouri and M. Noroozifar, *Anal. Bioanal. Chem. Res.*, 2018, **5**, 343–352.
60 A. B. Teradale, S. D. Lamani, P. S. Ganesh, B. E. Kumara Swamy and S. N. Das, *Sens. Bio-Sensing Res.*, 2017, **15**, 53–59.
61 C. V.Uliana, H. Yamanaka, G. S.Gerbellini and G. R.Salazar-Banda, *Quim. Nov.*, 2010, **33**, 964–967.
62 S. Ebrahimi, A. Afkhami and T. Madrakian, *J. Electroanal. Chem.*, 2019, **838**, 186–194.
63 S. Kim, N. Wang, Y. Li and X. He, *Anal. Methods*, 2016, **8**, 7780–7788.
64 P. Labroo and Y. Cui, *Analyst*, 2013, **138**, 1325–1328.
65 K. veerachar Harisha, B. E. K. Swamy, P. S. Ganesh and H. Jayadevappa, *Anal. Bioanal. Chem.*, 2018, **10**, 1273–1287.

View Article Online
DOI: 10.1039/D0AN01507E

Table of content

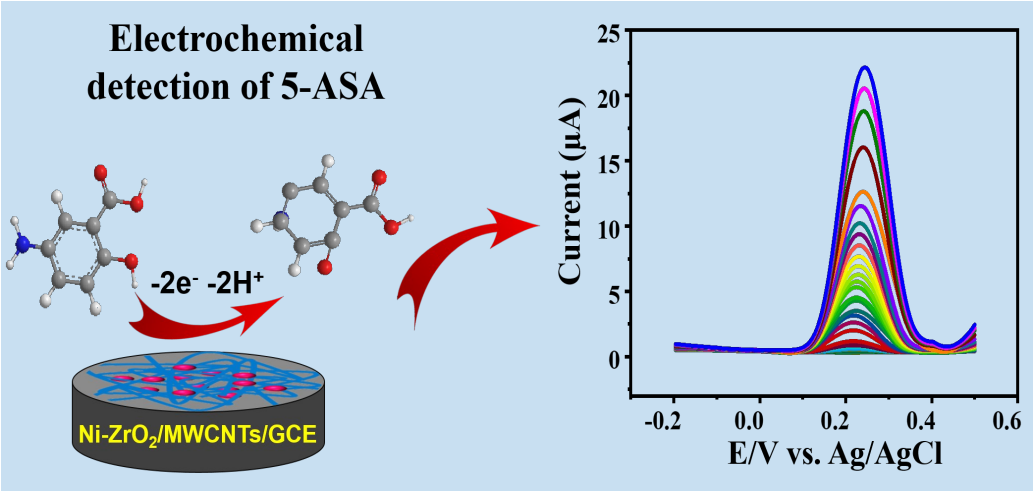

TOC illustrates that the fabrication of Ni-ZrO_2/MWCNT/GCE for highly sensitive electrochemical detection of 5-ASA in biofluids.